Bull Volcanol (2014) 76:833
DOI 10.1007/s00445-014-0833-7

RESEARCH ARTICLE

Physical weathering and modification of a rhyolitic hyaloclastite in Iceland

S. J. de Vet · M. C. Mittelmeijer-Hazeleger ·
J. J. M. Braakhekke · L. H. Cammeraat

Received: 22 January 2014 / Accepted: 9 May 2014 / Published online: 29 May 2014

Abstract Fragmental volcanic glass or 'hyaloclastite' is a common glaciovolcanic eruption product that is formed in large abundance during basaltic, andesitic and rhyolitic subglacial eruptions. The physical weathering of rhyolitic hyaloclastites differs notably from basaltic hyaloclastites due to differences in cementation and edifice consolidation. As rhyolitic glasses are also much rarer, comparatively little is known about their physical weathering and fracturing characteristics. In the presented study, we provide a process-oriented analysis of the physical modification of subglacially erupted rhyolitic hyaloclastites from the Bláhnúkur edifice in Torfajökull (Iceland). Frost weathering experiments were performed to determine how vesicular glass particles fragment to finer particle sizes. The surficial porosity of the glass drives such frost weathering through the process of pore pressurisation and was quantified using high-pressure mercury intrusion. Uniaxial compression experiments were carried out to understand how the glass structure responds to the application of external stress. The observed fracturing in both experimental treatments was found to adhere to fractal statistics, which allowed the compression experiments to be used in conjunction with the frost weathering experiments for inferring the fracturing characteristics of rhyolitic volcanic glasses. Transport processes by wind and gravity were simulated by long-duration abrasion experiments in rock tumblers (through granular avalanching), but these low-energy particle interactions were not found to significantly abrade particles. A notable result from our fragmentation experiments was the production of <10 μm particles. This size range is considered respirable and illustrates how physical weathering can continuously create potentially harmful ash textures; a process which is often overlooked in health hazard assessments after volcanic eruptions. Fragmentation by post-eruptive weathering can lead to overestimations of the fine ash fraction produced by syneruptive fragmentation and granulometric studies therefore need to be appreciative of the effects of such secondary fracturing processes.

Keywords Glaciovolcanism · Volcanic glass · Volcanic ash · Rhyolite · Fractal fracturing · Porosity · Ice · Transport · Health

Introduction

Volcanism coinciding with the glaciation of volcanic provinces leads to the formation of fragmental volcanic glass known as *hyaloclastite*. It is found in basaltic, andesitic and rhyolitic variants, each with different chemical alteration characteristics that affect their present-day physical weathering. The formation of hyaloclastite facies has been linked to subglacial volcanism since the early pioneering work in Iceland by Pjetursson (1900) and Peacock (1926). Edifices composed of these materials are commonly recognised after deglaciation as *tindars*, and these linear ridges are common features along Iceland's volcanic rift zones (Jakobsson and Gudmundsson 2008; Russel et al. 2014). Their generic lithofacies comprise a basal pedestal composed of pillow lavas, which is superposed by the glassy hyaloclastite breccias (Chapman et al. 2000; Schopka et al. 2006; Jarosch et al. 2008). For basaltic eruptions, the transition from pillow lavas to hyaloclastite is in

Editorial responsibility: M. Manga

S. J. de Vet (✉) · J. J. M. Braakhekke · L. H. Cammeraat
Earth Surface Science, Institute for Biodiversity and Ecosystem Dynamics, University of Amsterdam, Science Park 904, 1098 XH Amsterdam, The Netherlands
e-mail: s.j.devet@uva.nl

M. C. Mittelmeijer-Hazeleger
Heterogeneous Catalysis and Sustainable Chemistry, Van't Hoff Institute for Molecular Sciences, University of Amsterdam, Science Park 904, 1098 XH Amsterdam, The Netherlands

principle controlled by the eruption cavity pressure, which changes the eruption style to an explosive type where volcanic glass is formed by fragmentation and rapid quenching (thermal contraction and shattering) of the erupting magma (Tuffen 2007). This fine-grained basaltic glass is easily chemically weathered and becomes cemented by the formation of palagonite (Nesbitt and Young 1984; Gislason and Oelkers 2003; Frolava 2008). Observations of palagonisation during the 1963–1967 Surtsey eruption (Jakobsson 1978; Jakobsson and Moore 1986) and estimates from the 1996 Gjálp eruption (Jarosch et al. 2008) suggest that cementation and consolidation of an edifice occurs within the first 1–2 years after eruption. In the case of mesa-shaped *tuyas* (Mathews 1947; Jones 1969, 1970; Russel et al. 2014; Smellie 2006; van Bemmelen and Rutten 1955), consolidation by palagonisation is able to transform these volcanic constructs into resistant features that can provide insights in the timing and thickness of past glacial ice sheets (Walker 1965, Licciardi et al. 2007). There are, however, appreciable differences between eruption products formed by basaltic and rhyolitic subglacial volcanism.

Compared to basaltic subglacial volcanism, rhyolitic subglacial volcanism is much rarer in Iceland, and it has been linked to 23 (suspected) locations, many of which still require further exploration (McGarvie 2009). The exchange of heat with the surrounding ice combined with differences in subglacial channelization of meltwater differentiates the dynamics of rhyolitic subglacial eruptions from their basaltic counterparts (Tuffen et al. 2002a, b). In spite of such differences, lithofacies formed by rhyolitic subglacial volcanism are comparable to those found in basaltic edifices and this also includes the abundance of fragmental volcanic glass (Tuffen et al. 2001, 2008). Chemical weathering of rhyolitic volcanic glasses occurs through the process of perlitisation, yet it does not lead to cementation and consolidation (Denton et al. 2009). This lack of edifice strengthening is the fundamental difference between rhyolitic and basaltic edifices and this makes deposits of rhyolitic volcanic glass much more susceptible to post-glacial erosion processes. However, studies of edifice erosion are scarce (Jakobsson and Gudmundsson 2008), and they are often limited to describing general geomorphic processes (e.g. Whalley et al. 1983; Schopka et al. 2006, Hartmann et al. 2003) with little focus on the modification of individual glass fragments. These modification characteristics are relevant for understanding edifice evolution, pedogenesis (Arnalds 2010; Arnalds et al. 2001, 2012) and the production of new particle-size classes that may increase respiratory health hazards (e.g. Horwell and Baxter 2006). Our modest understanding of the environmental fate of rhyolitic hyaloclastites emphasises the need for further research. The aim of this study is to provide a process-oriented analysis of hyaloclastite modification by integrating experiments of frost weathering and particle transport. We address the effect of these processes for glass fragments that comprise the hyaloclastite facies of the well-studied rhyolitic edifice Bláhnúkur in Torfajökull (Iceland).

Frost weathering

The rate of chemical weathering is low in cold periglacial conditions and this increases the relative contribution of physical weathering (Peltier 1950). Periglacial refers in this case to the cold environments where geomorphic processes in top soils, sediments and exposed rock faces result from the freezing of water. At the interface of rhyolitic hyaloclastites with the local environment, the conditions for the physical weathering by volumetric expansion of ice (i.e. frost heave) are ideal. The low cohesive strength and lack of cementation allow water derived from snow melt and rain to saturate the upper few centimetres of exposed hyaloclastite. Freezing in this zone of the rock face is often rapid enough to heave and detach individual particles (Matsuoka and Murton 2008). Ice has the unique property of expanding 9 % in volume during freezing, which can generate a stress inside a material that can exceed the maximum fracturing strength by several orders of magnitude (Matsuoka and Murton 2008). This form of *external damage* is mainly relevant near the surface and it is of lesser importance deeper inside the rock (<10 cm) due thermal dampening effects (Hinkel 1997). Freezing of water occurs at nucleation points that are often small (nanometre- to micrometre-sized voids at the surface of a particle) and they fulfil an important role in the frost weathering of these materials (Scherer 1999; Walder and Hallet 1986). While the semantics of *pore* differs per scientific discipline, we use this term to encompass all nanometre- to micrometre-sized voids at a particle's exterior. These pores either result from processes related to magma vesiculation and gas exsolution, or from post-eruptive chemical weathering (i.e. perlitisation; Denton et al. 2009). Ice nucleation can generate stress inside pores with diameters above 5 nm (Scherer 1999), but most relevant for the processes discussed in this work are pore diameters >100 nm. Above this size limit, ice is capable of growing from the outside into a pore. As the ice front intrudes deeper into the water-saturated void, it builds up a hydrostatic pressure (Scherer 1999; Scherer and Valenza 2005). Fracturing by such pore pressurisation (*internal damage*) occurs when the generated stress field exceeds the dimensions of the nearest largest flaw (Scherer and Valenza 2005). In other words, when stress is generated in a pore or a pore network with a stress field that has a length scale D, propagation of a fracture is only possible if the length of the fracture is $<D$. Several freeze–thaw cycles are often needed to produce enough damage to induce wide-spread fracturing of a material (Matsuoka and Murton 2008).

Down-slope transport

Another way in which individual particles can be modified is by transport processes. Such effects have been shown for pyroclastic density currents (Manga et al. 2011; Kueppers et al. 2012) and in volcanic and fluviatile debris flows (Kaitna and Rickenmann 2007; Caballero et al. 2012). For poorly cohesive deposits such as rhyolitic hyaloclastites, modification may also result from geomorphic agents such as the wind. Modification during aeolian processes is principally driven by particle impacts (Greeley and Iversen 1985; Marshall et al. 2012) that results from transport along ballistic trajectories in a process known as *saltation* (Bagnold 1954). Saltation has an impact regime of 1–10 m s^{-1} (Marshall et al. 2012), which makes it an efficient process for particle modification as shown in experimental studies by Merrison et al. (2010) and Marshall et al. (2012). However, this process is dominant for the modification and segregation of materials on flat terrains such as Iceland's sandy deserts (Arnalds 2010; Arnalds et al. 2001, 2012; Mangold et al. 2011; Leadbetter et al. 2012); it will occur infrequently on the steep slopes of tuyas and tindars where it is difficult to achieve saltation. Low-energy particle interactions during wind-induced, down-slope rolling and inside gravity-driven granular avalanches will therefore encompass a substantial part of the particle interactions at the flanks of subglacially formed edifices.

In this study, the two processes outlined above are experimentally studied to establish how they contribute to the modification of hyaloclast fragments at Bláhnúkur. The excellent accessibility and unique geological setting of the Bláhnúkur edifice in Torfajökull (Iceland) make it the best-studied rhyolitic subglacial edifice globally. This also provides a well-defined case for studying the physical weathering and modification of rhyolitic hyaloclastites.

Bláhnúkur in Torfajökull, Iceland

Bláhnúkur was formed 115−11 ka ago in the Weichselian glacial phase and is one of the youngest glaciovolcanic landforms in the Torfajökull caldera complex (Tuffen et al. 2001), which is presently part of the Fjallabak Nature Reserve. The area is situated in the southern central highlands of Iceland at the intersection of the Veiðivötn fissure swarm and the caldera complex (Fig. 1). The small-volume (<0.1 km^3) effusive eruption formed a hyaloclastite layer of several tens of meters thick that covers an older rhyolite core (Tuffen et al. 2001; McGarvie et al. 2006), and this makes the edifice an atypical tindar. Bounding Bláhnúkur to the north is the *Laugahraun* lava flow, which formed by a comparable subaerial eruption in 1477 AD. Both erupted volumes of Bláhnúkur and Laugahraun show signs of the mixing of basaltic magma in the rhyolitic ground mass of Torfajökull (Blake 1984; Tuffen et al. 2001). Millimetre and even centimetre-sized basaltic inclusions in the hyaloclastite matrix evidence the pre-eruptive intrusion and breakup of a basaltic magma body that likely promoted both eruptions. This mechanism explains well why tuya-forming eruptions in Torfajökull, unlike other parts in Iceland, appear to be dissociated from lithosphere unloading effect during deglaciation of the area (Jull and McKenzie 1996; Slater et al. 1998; Maclennan et al. 2002; McGarvie et al. 2006; McGarvie 2009). The pyramid-shaped edifice currently rises 350 m above the surrounding rhyolite plateau to a summit altitude of 945 m.a.s.l. Local palaeo-ice thicknesses have been inferred using geologic features (Tuffen et al. 2001) and nearby similar-aged tuyas (Tuffen et al. 2002a). These features indicate that the area was covered by an ice sheet of at least 350–400 m thick at the time of eruption. This glacial thickness was later corroborated using the volatiles sequestered in the glass, which were correlated to the confining eruption cavity pressure (Tuffen et al. 2010; Owen et al. 2012). The emplacement of the subglacial eruption products and the lava lobe-hyaloclastite facies were first described by Furnes et al. (1980) and substantially improved by Tuffen et al. (2001). The latter proposed a highly dynamic eruption environment where glacial recession triggered mass movements (i.e. sliding and slumping) that contributed to the strata presently exposed on the flanks and in the gorges around the edifice. The subglacial eruption of Bláhnúkur took place inside a melt-water dominated subglacial cavity where rapid degassing, spalling and shattering led to the formation of hyaloclastites (Owen et al. 2012). These materials are characterised by a poorly sorted, mesokurtic medium to fine ash matrix with percentile particle diameters of D_{50}=297 µm and D_{90}=1,255 µm (de Vet and Cammeraat 2012) with larger, centimetre-sized vesiculated fragments with 10–20 % of vesicles in excess of 1 mm in diameter (Owen et al. 2012). Recent geochemical studies of the Bláhnúkur hyaloclastites have addressed the chemical weathering of rhyolitic glass through the process of perlitisation (Denton et al. 2009, 2012) and changes in magnetic properties due to progressive post-eruptive hydration (Ferk et al. 2012). In this study, we focus primarily on physical weathering processes that affect the freshly excavated hyaloclastites inside *Grænagil*, a roughly 2 km long NE-SW trending gorge on the north flank of Bláhnúkur. The gorge formed after 1477 AD, when local streams had to re-establish their flow paths in response to the Laugahraun eruption that blockaded the pre-eruptive valley (de Vet and Cammeraat 2012). The incision of the Brennisteinsöldukvísl stream at the interface of the resistant subaerial lava and the softer Bláhnúkur hyaloclastite has produced a ~30-m deep gorge of variable width due to the meandering nature of the stream. Funnelling of local wind flow in this gorge creates a 'wind tunnel' effect where wind

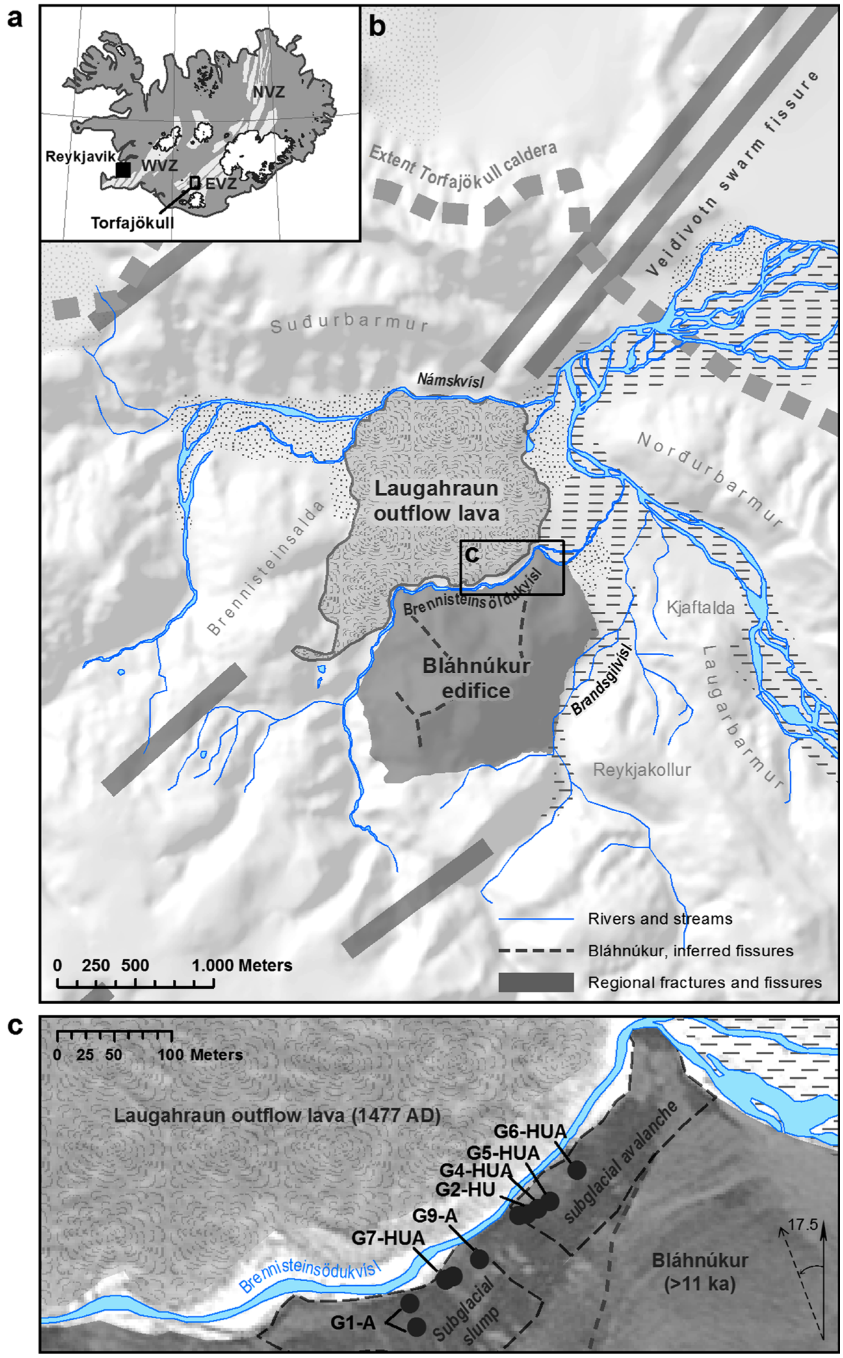

Fig. 1 Overview of the Bláhnúkur region near the intersection of the Torfajökull caldera and the Veiðivötn fissure swarm on the edge of the Eastern Volcanic Zone (EVZ) and Southern Flank Zone (SFZ) in Iceland (**a**); fissure data, Einarsson and Sæmundsson (1987). The study area in the southern central highlands (**b**) is dominated by migration of local hydrological networks and the narrow incision of the stream after the Laugahraun eruption. Fissures and emplacement units are based on Tuffen et al. (2001). Sampling sites of hyaloclastites are indicated in (**c**) where the last letters highlight their experimental treatment in this study; *H* = high-pressure mercury intrusion, *U* = uniaxial compression, *A* = abrasion experiments. Maps adapted from de Vet and Cammeraat (2012)

speeds easily reach threshold conditions to deflate fine ash from the hyaloclastite outcrops and sediments (de Vet and Cammeraat 2012). In absence of long-term meteorological records on site, indications from nearby meteorological stations (Table 1) show that the local climate in this remote part of Iceland is favourable for periglacial processes. These processes may be further promoted by the northern exposure of the Grænagil gorge, which shelters the slopes from solar

Table 1 Meteorological overview of field conditions in the central highlands of Iceland

Thermal conditions	Year				
	2007	2008	2009	2010	2011
Vatnsfell					
Mean annual temperature [°C]	1.1	1.1	1.8	1.8	1.8
Minimum recorded temperature [°C]	−16.9	−21.8	−16.1	−17.3	−17.9
Maximum thermal gradient [°C min^{-1}] [a]	0.13	0.13	0.17	0.19	0.05
Days of freezing	159	165	130	144	106
Freeze–thaw cycles	144	62	117	86	116
Lónakvísl					
Mean annual temperature [°C]	0.6	0.3	0.7	1.0	0.6
Minimum recorded temperature [°C]	−19.0	−21.8	−19.2	−20.2	−20.3
Maximum thermal gradient [°C min^{-1}] [a]	0.15	0.09	0.16	0.16	0.10
Days of freezing	167	173	153	151	158
Freeze–thaw cycles	127	67	125	93	129
Melting of snow cover[b] [day–month]	7–6	29–6	5–6	2–6	21–6
New snow cover[b] [day–month]	–[c]	–[c]	30–9	–[c]	–[c]

In the absence of meteorological records and stations near Bláhnúkur, the nearest stations located in Vatnsfell (539 m.a.s.l., at 24 km) and Lónakvísl (675 m.a.s.l., at 26 km) provide an order of magnitude for the microclimate inside the Grænagil gorge at the base of Bláhnúkur. Table modified from de Vet and Cammeraat (2012)

[a] From hourly temperature measurements

[b] Based on F208 road access to Landmannalaugar; data from Vegagerðin (Icelandic Road Administration)

[c] Not measured or no data available

insolation and prevents large diurnal temperature fluctuations in favour of periglacial processes. Amongst the variety of geomorphic processes that cause erosion inside the gorge de Vet and Cammeraat (2012) identified frost weathering and wind erosion as the two most notable processes that lead to the breakup of the hyaloclastite and the transport of glass fragments. The occurrence of these two processes provides the rationale for the experimental treatments of the rhyolitic hyaloclastites discussed in this study.

Experimental approach

The focus of our experimental approach was the quantification of physico-mechanical properties to understand their relation with the physical modification of individual particles. The first part of this methodological paragraph will address the collection of samples inside the Grænagil gorge, which were used in four different types of experiments. The description of these experiments is divided into two sections; the first part focuses on experiments used to understand frost weathering; the second addresses the effects of particle transport on the flank slopes by wind and gravity. Figure 2 provides an illustrated overview of our experimental approach and the used work flow.

Sample collection

Outcrops of moderately consolidated hyaloclastites were sampled to depths of 10 cm, where according to Hinkel (1997), the largest effects of freeze–thaw cycles are expected as a result of thermal diffusion and water infiltration. Their locations are marked in Fig. 1c. At each sample site, a 1 dm^3 block of hyaloclastite was excavated (Fig. 2a) such that a sample was obtained from the hyaloclastites and not from the remobilised materials that compose the underlying sedimentary units (Fig. 3). While samples were taken in close proximity to each other, three different slope sections can be identified. Section A (Fig. 3a; sample G6-HUA) is a bright-green hyaloclastite outcrops that has a fine-grained ash matrix characterised by interwoven veins composed of silt-sized ash. Tuffen et al. (2001) interpreted these veins as a result of steam filtering through the hyaloclastite, which deposited the fines in the joints between larger hyaloclastite blocks. In their interpretation, this section of Bláhnúkur was formed by a hot avalanche inside the subglacial eruption cavity. Larger vesicular fragments are set in this fine-grained matrix and generally compose ~10–20 % of the total volume (inset next to Fig. 3a). Section B (Fig. 3b; samples G2-HU, G4-HUA and G5-HUA) is situated directly adjacent to section A, and it is characterised by a paler grey colour and partly underlies the green hyaloclastites from section A. The ash matrix includes basalt

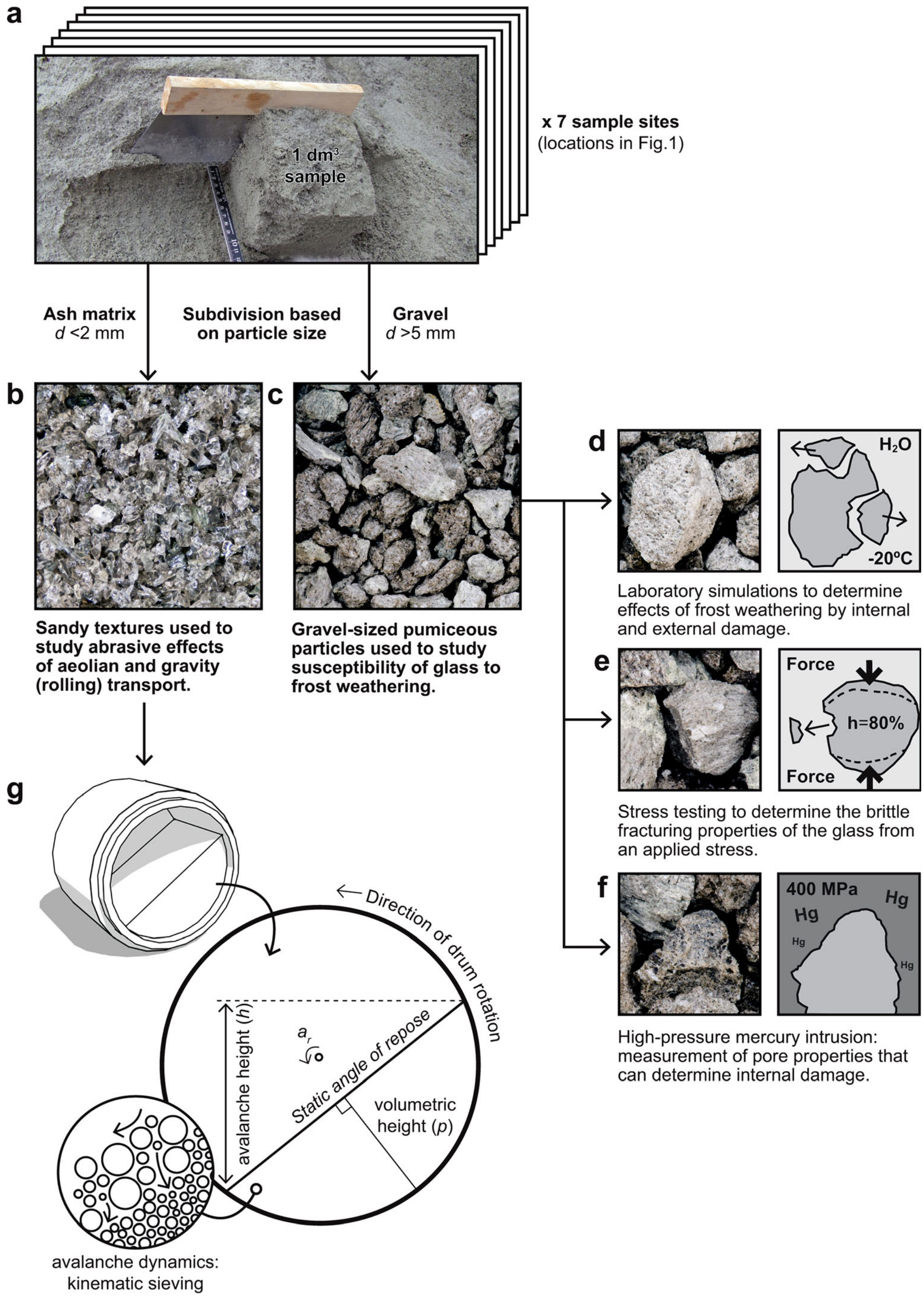

Fig. 2 Illustration of the process-oriented experimental protocol used in this study. Cubic decimetre samples (**a**) were collected at the sample sites (also see Figs. 1 and 3). As transport and frost weathering depend on particle diameters, samples were subdivided into sand-sized (**b**) and gravel-sized vesicular subsamples (**c**). The latter size range was selected as it contains microscopic pores at the glass surface and larger pores in the form of vesicles. This makes these particles ideal for studying internal and external fracturing processes (see the "Introduction" section for the distinction). Individual vesicular particles were subdivided into three experiment groups to measure **d** the damage caused by frost weathering, **e** the response of the glass to brittle deformation and **f** the pore diameters. Experiments (**e**) and (**f**) were used to interpret the new particle-size classes formed in experiment **d**. Finally, sandy textures that are most susceptible to gravity-induced and wind-induced rolling were studied using a rotating drum set-up (**g**)

fragments and the lack of veins filled with fine ash sets this section apart from the green 'avalanche deposits'. It is characterised in the description of Tuffen et al. (2001) as an unmodified hyaloclastite deposit. Section C (Fig. 3c, samples G1-A, G7-HUA, and G9-A) is generally comparable to section B and also contains basaltic inclusions several millimetres to centimetres in size. This slope section of Bláhnúkur is characterised by a larger amount of lava lobes and was interpreted by Tuffen et al. (2001) to be formed by a slumping event. Granulometric analyses by de Vet and Cammeraat (2012) show that the ash matrices of collected samples are comparable (percentile diameters are given in Fig. 3), and they can be classified as poorly sorted, mesokurtic medium to fine ashes, based on the arithmetic method of moments from Friedmann and Sanders (1978).

Experiments of frost weathering

Many fragmentation processes in geology have been shown to be scale invariant and adhere to fractal statistics (Turcotte 1986; Perfect 1997) and a notable application of fractal statistics is to the formation of pyroclasts (Kueppers et al. 2006; Perugini and Kueppers 2012). The use of fractals (i.e. Mandelbrot 1975, 1982) can therefore provide a statistical approach to characterise the relation of the size and amount of fragments formed during fracturing of heterogeneous materials (Perfect 1997). A general fractal relation is a power law in the form of $N \propto d^{-f}$, where N is the amount of fragments of a diameter d, with f as the fractal dimension (Turcotte 1986, 1989). In the case of fracturing of brittle of quasi-brittle materials, fragment sizes were found to be proportional to the dissipation of energy from the applied stress (Carpineri and Pugno 2002). If a fragment distribution has a fractal dimension, then it can be considered as a measure of the material's resistance to fracturing, evidencing a scale invariant fracturing process (Turcotte 1986). We aimed at comparing the fragmentation in two physically different processes (frost weathering vs. uniaxial compression) using the fractal properties of the formed particle-size distributions as a basis for inferring the fracturing characteristics of hyaloclastite. As a full analysis of fractal properties exceeds the aim of this paper, we limited the analysis to calculating only the fractal dimension for the number distributions. To this end, we calculated the number of fragments (N) from their volumetric abundance in an arbitrary volume and then fitted the aforementioned power law $N \propto d^{-f}$ to the obtained number distribution. If the number distributions in both experiments poses fractal properties, and in addition, have comparable grains size distributions, then it would signify comparable energy dissipation by the glass structure in both our experimental treatments of the volcanic glass (Carpineri and Pugno 2002).

Laboratory freeze–thaw cycles

Laboratory simulations of frost weathering were carried out using the samples described above to assess the damage caused by freezing of hyaloclast particles with water. In these experiments, gasket-sealed tubes of 50 ml were filled with 1.5 g of vesicular particles (2–3 in total) and 1.0 ml water was added to saturate the particles by capillary rise in vesicle networks and/or by full immersion (Fig. 2d). The sealed tubes (with a repetition of n=12 per sample site) were frozen to −19 °C inside a freezer. According to the Gibbs–Thomson equation, the freezing point is suppressed to −12 °C inside the smallest pores in which ice can nucleate (5 nm; Scherer and Valenza 2005). The low temperatures used in the experiments are, therefore, sufficiently far below freezing to assure that ice also infiltrated in the smallest surface pores such that stress was generated at all pore scales. The used temperatures simultaneously match the order of magnitude of temperature extremes in the field (Table 1). After 16 h of freezing, particles were thawed over 8 h at +5 °C, and this sequence was repeated for 10 cycles. The exposure to consecutive freeze-thaw cycles induced fracturing of the vesicular particles which produced new particle-size classes (see Fig. 4). The <1,400 μm (sieve size) particles formed in the 12 tubes were homogenised into a single sample and pre-treated with an $Na_4P_2O_7.10H_2O$ dispersing solution to bring the finest particles into suspension (Eshel et al. 2004). Particle-size distributions of the fragments were subsequently measured using a Sympatec HELOS laser-diffraction particle sizer. As samples were frozen in conditions that can lead to both internal and external damage, two experiments were subsequently carried out to help interpret the observed fragmentation in these frost weathering experiments.

Uniaxial compressive strength

Fracturing of volcanic glass during frost weathering is dominated by the stress that is generated within the exterior surface pores of a glass fragment (Scherer and Valenza 2005). It is currently unfeasible to directly quantify the magnitude of stress inside the glass or the direction and magnitude of forces created during ice nucleation inside these nm-μm sized pores during frost cycling. Using an experimental method in which this stress can be controlled may alternatively be used to obtain insight in the fracturing behaviour of vesicular hyaloclast fragments. Tensile and compression tests are common methods for measuring the fracturing characteristics of a material and they quantify parameters such as stress (σ, force per area) strain (ε, deformation) and strain rate (deformation per time step) using standardised sample geometries. However, this approach is for many practical reasons not possible with vesicular hyaloclasts as a standardised contact area cannot be produced due to the friable nature of these particles. Although other studies have shown the relation of compression with tensile properties of non-vesiculated rocks (e.g. Hiramatsu and Oka 1966; Rocchi et al. 2002), we used a different approach for analysing the obtained force signal during compression of rock specimen. Fragmentation experiments were performed using an M359-20CT test bench from Testometric under ambient room temperature conditions such that fracturing was brittle as under field conditions (Fig. 2f).

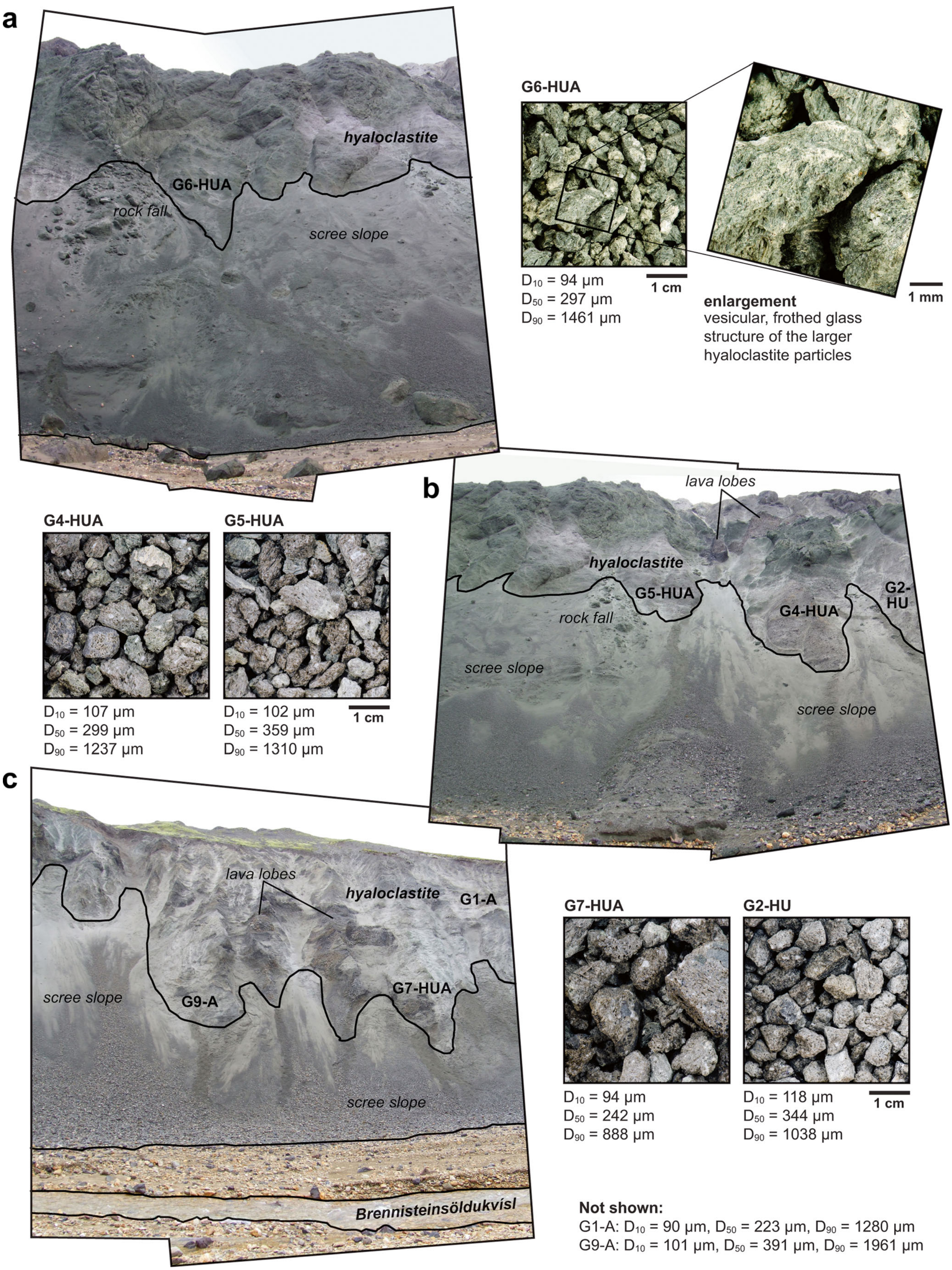
a
hyaloclastite
G6-HUA
rock fall
scree slope
G6-HUA
D_{10} = 94 µm
D_{50} = 297 µm
D_{90} = 1461 µm
1 cm
1 mm
enlargement
vesicular, frothed glass structure of the larger hyaloclastite particles
G4-HUA
D_{10} = 107 µm
D_{50} = 299 µm
D_{90} = 1237 µm
G5-HUA
D_{10} = 102 µm
D_{50} = 359 µm
D_{90} = 1310 µm
1 cm
b
lava lobes
hyaloclastite
G5-HUA
G2-HU
G4-HUA
rock fall
scree slope
scree slope
c
lava lobes
hyaloclastite
G1-A
scree slope
G9-A
G7-HUA
scree slope
Brennisteinsöldukvísl
G7-HUA
D_{10} = 94 µm
D_{50} = 242 µm
D_{90} = 888 µm
G2-HU
D_{10} = 118 µm
D_{50} = 344 µm
D_{90} = 1038 µm
1 cm
Not shown:
G1-A: D_{10} = 90 µm, D_{50} = 223 µm, D_{90} = 1280 µm
G9-A: D_{10} = 101 µm, D_{50} = 391 µm, D_{90} = 1961 µm

◀ **Fig. 3** Stitched context photos of the sampled slope sections inside the Grænagil gorge. Notable features are listed and samples were collected from the original hyaloclastite facies situated above local scree sediments. These features are formed by the weathering of the exposed hyaloclastite and consist of fine-grained material that comprises the ash matrix of the hyaloclastite. Images accompanying the context photos are focus-stacked microscope images of large vesicular particles used in the frost weathering experiments. Particle size distribution (percentile diameters) given for the hyaloclastite ash matrixes are taken from textural analyses by de Vet and Cammeraat (2012)

Similar vesicular glass particles as used in the frost weathering experiments were compressed between two flat loading platens to 80 % of their original height (with n=9 independent repetitions). Measurements of the compression force were obtained with an accuracy of 10^{-2} N at a constant strain rate of 5.8 μm s^{-1}. The *force*–strain data from the compression tests were then analysed, as opposed to more commonly used *stress–strain* data. The measured force (i.e., a signal with changing frequency and amplitude) was treated as the sum from an unknown amount of contact points that resist the applied deflection up to a magnitude beyond which the internal stress becomes too great and brittle failure occurs. Fast-Fourier-Transform (FFT) analyses of the force signal were therefore used to calculate the most commonly occurring deflections that caused the vesicular glass to fracture. These FFT analyses produce 'periodograms' in which peaks represent the frequently reoccurring deflections that lead to failure of the vesicular glass structure. Plotting of these peaks collectively in a box plot made it possible to compare of the range of these 'critical deflections' for each of the sample sites. The granulometries of the <1,400 μm fragments formed by uniaxial compression were subsequently measured according to the same procedure as in the frost weathering experiments.

Pore properties using mercury porosimetry

Porosimetry is an analytical technique used to describe the pore properties of a material. In the analyses of frost weathering characteristics, porosimetry of hyaloclast fragments is particularly valuable as it allows us to understand the aptitude of the glass for *internal damage* from pore pressurisation. A common and accurate method to quantify pore properties is by high-pressure mercury intrusion (Rouquérol et al. 1994; Sing et al. 1985). Mercury has the property that it will not infiltrate into pores via capillary action due to the high surface tension of the metal (Good and Mikhail 1981; Rouquérol et al. 1994). Infiltration can therefore only be achieved at a pressure (P) that is proportional to the diameter of a pore (D), and it is given by the Washburn equation in the form of $D=-2\gamma\cos\theta/P$ (León y León 1998). Here, θ is the contact angle (140°) and γ the surface tension (485 mN m^{-1}) of mercury (Good and Mikhail 1981). The infiltration of mercury into large pore diameters (~μm) will, therefore, require a lower pressure compared to very small pores (~nm). Quantifying the volume change in mercury at a given pressure makes it possible to obtain a reliable measure of the glass' pore properties, which is always based on the minor axis of the pore. We measured the porosity of bulk samples consisting of ten ~0.25 cm^3 vesicular particles with n=9 independent repetitions for 5 sample locations (Fig. 2e). These measurements were made using a PASCAL 440 porosimeter from Thermo following the DIN 66133 standard for mercury intrusion measurements. The measurements were carried out under pressures of 0.1–400 MPa that allowed us to quantify pore diameters of 3.75 nm–15 μm. Combined with the measured bulk and vesicle-free skeletal densities (ρ_{He}), it also allowed us to quantify several generic porosity parameters (e.g. pore volume, (in) accessible porosity and specific surface area). Obtained pore properties of the Bláhnúkur hyaloclastite were statistically compared using an analysis of variance (n-way ANOVA at the p=0.05 significance level) to analyse if these properties are a common property of the Bláhnúkur particle population or unique for the sampled location.

Particle abrasion experiments

The abrasion of granular sediments during transport was experimentally simulated using continuous axial tumbling. Such set-ups have been used for understanding abrasive effects in pyroclastic density currents (Kueppers et al. 2012) and debris flows (Kaitna and Rickenmann 2007; Caballero et al. 2012) and for assessing the susceptibility to abrasion based on the degree of quenching (Patel et al. 2013). The abrasion of the angular glass particles by low-energy transport processes was studied using six rubber-covered rock tumblers with a 10-cm diameter that rotated at 50 rpm (300°/s). We used this set-up (Fig. 2g) as a simplified model for the observed sediment transport in summer months by wind-induced and gravity-induced processes. The abrasion experiments were performed with a sieved size range of 300–600 μm which comprises part of the main mode of the ash matrix (de Vet and Cammeraat 2012). Numerical simulations of granular avalanche velocities inside similar rotating drums show that particles collide at 0.3 m s^{-1} (Yang et al. 2008), well below the high-energy impact regime of saltating gains (1–10 m s^{-1}, Marshall et al. 2012). In rotational set-ups unmixing effects from axial segregation (Aranson and Tsimring 2006) would bias larger particles over smaller particles in their transported distance over time. We therefore filled the drums below the axis of rotation (a_r, Fig. 2g) to overcome this problem and this ensured that aliquots taken from the sediment were properly mixed and representative of the transported sediment in the tumblers. Indications from past tumbling experiments with vesiculated materials suggest that the highest degree of fracturing occurs in the first week or even hours (Kueppers et al. 2012; Manga et al. 2011; Patel et al. 2013). We therefore had a

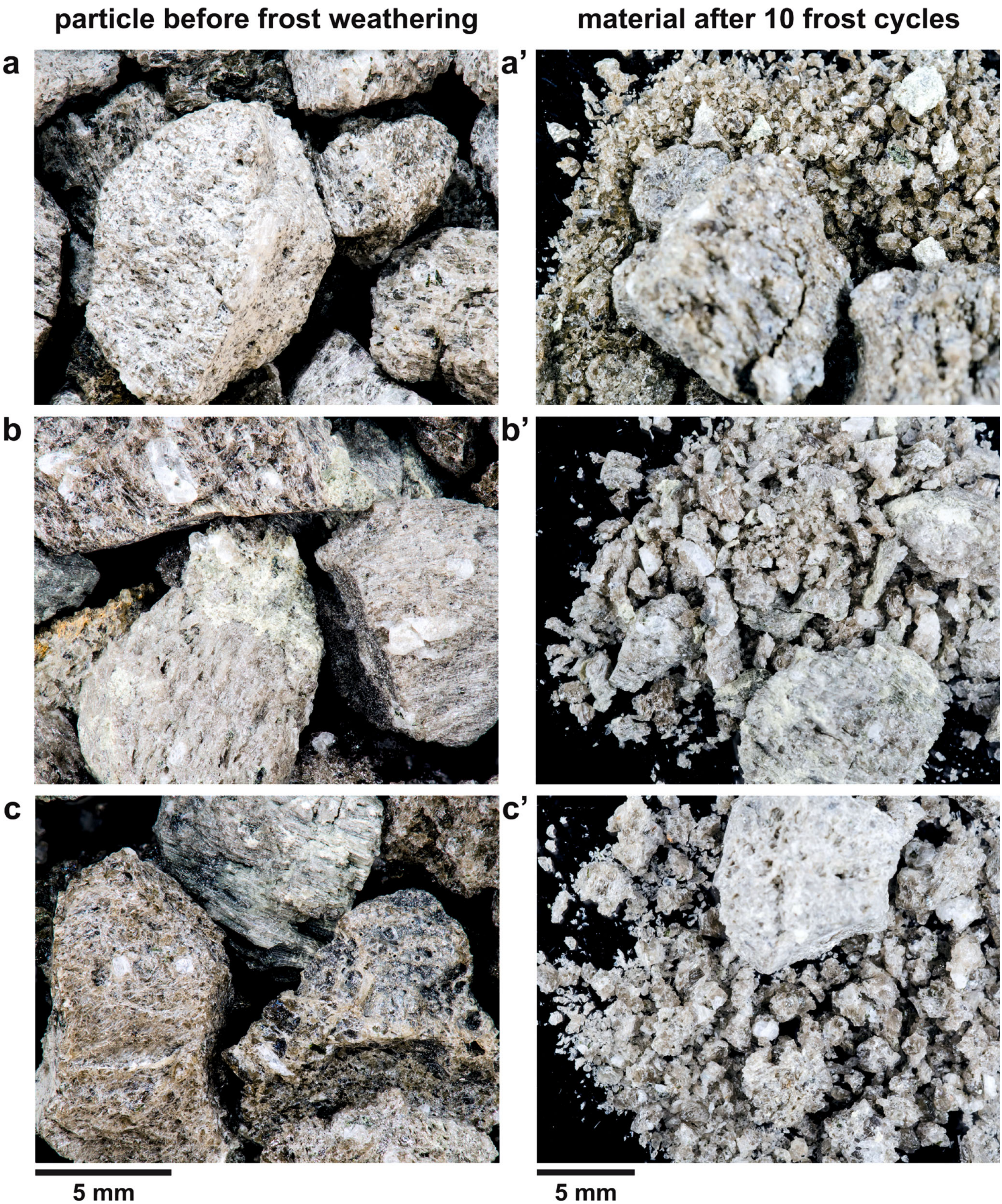

Fig. 4 Comparison of the large vesicular particles used in the frost weathering experiments and uniaxial loading tests. The *left column* (**a**–**c**) shows examples of intact particles from G2-HU, G4-HUA and G7-HUA, respectively, before the experiments started, while the *right column* (**a'**–**c'**) shows the new particle size classes formed after fracturing of an individual particle. Fragmentation during uniaxial compression of individual particles resulted to comparable particle size distributions <1,400 μm, which are compared in Fig. 5

weekly sample rate during the first five weeks of tumbling and we continued the experiment for a total of 15 weeks. After each week of tumbling, a ~15-g aliquot was extracted from the bulk to measure changes in the granulometry according to the same procedure as in the experiments described above.

Results

Frost weathering of individual vesicular particles was found to induce wide-spread fracturing which produced new particle-size distributions (Fig. 4). The granulometry of the newly formed, smaller particles are predominantly coarse sandy textures, evidenced by the mode around 300–900 μm (Fig. 5a, black curves). A notable feature in the granulometry of the fracturing products is the distinctive mode <10 μm. When comparable vesicular particles were compressed between rigid loading platens, we obtained very similar granulometries to the frost weathering experiments (Fig. 5a, blue curves). Here, too, two modes were found with the primary mode at 300–900 μm, and a much smaller secondary mode <10 μm. The particle-size distributions were converted into their number distributions and found to plot on a line (Fig. 5b) which adheres to a power law with a fractal dimension of f=2.1.

A more detailed information on the fracturing process during compression was obtained in the analysis of the force-strain signal (Fig. 6a), which was characterised by numerous small peaks. Each peak represents a build-up of force which suddenly decreased as the glass fractured; i.e. the force resisting the applied strain (deflection) reduced when the glass structure failed. This highly variable signal of successive fracturing events is superimposed on a lower frequency, larger amplitude signal that may represent the effects of the changing contact area during compression (Fig. 6a). Frequency analyses, therefore, allowed us to extract the recurring critical distances at which fracturing took place, visible as peaks marked by blue triangular markers in the periodograms (Fig. 6b). After normalisation,, we extracted these peaks based on a relative threshold of 0.01 % with surrounding data points. The interquartile range (i.e. middle 50 %) of critical deflections was found to cover a range of 25–75 μm (Fig. 6c). A statistical inspection of the peak distribution using the box plots suggests that the notches of the boxplots and medians are not statistically different. This indicates that the critical deflection range of 25–75 μm is comparable for all the particles, independent of the sampled site.

Measurements of the surface porosity of hyaloclastite fragments are shown in Fig. 7 where a normalised value of the pore ($dV/d\log D$) is plotted against the pore diameter (D). Each curve is the average of 9 independent measurements with 10 different fragments (i.e. 90 vesicular fragments were measured per site). We found that the porosity is in all cases bimodal, evidenced by a narrow peak at ~3,000 nm and broader peak centred at ~5,000 nm. The green hyaloclastites located at site G6-HUA were notably different as these had a trimodal distribution with the additional mode centred on ~700 nm. Other particle properties and pore properties quantified using mercury porosimetry are summarised in Table 2. Based on a statistical analysis of variance (i.e. n-way ANOVA tested at the 5 % significance level) of all individual measurements, we established that of the various pore properties listed in Table 2, the modal pore diameters and inaccessible porosity are comparable and as such site-independent properties of the glass. The inaccessible porosity is calculated using the skeletal and envelope densities from Table 2, and it represents the pores that are accessible to helium, yet whose diameter are too small for mercury to infiltrate.

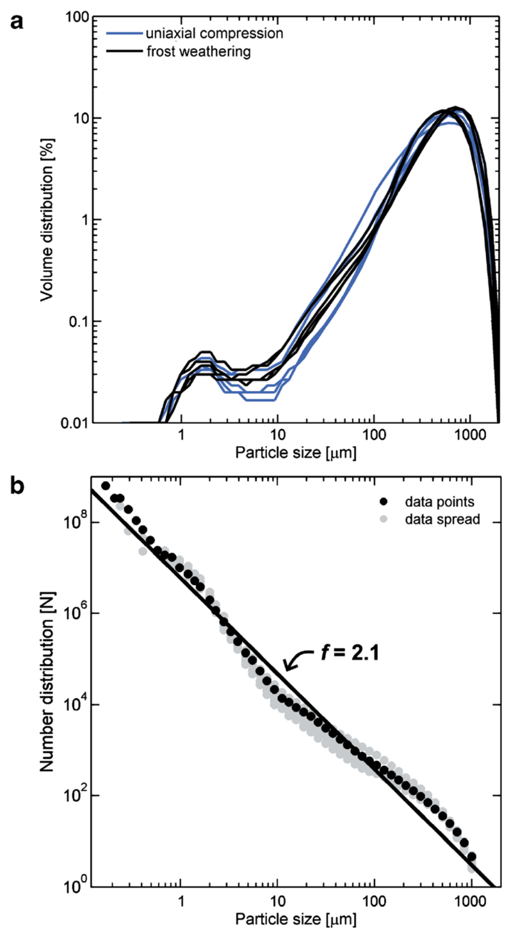

Fig. 5 Volume and number distributions formed by glass fragmentation. New particle size classes (**a**) produced by fracturing of individual vesicular particles with diameters of d >5,000 μm. Effects of frost weathering (10 cycles) produced a decay to finer particle-size classes shown here in *black*. Comparable particle classes were formed when identical particles were subjected to uniaxial loads (in *blue*) that induced brittle fracturing of the vesicular glass structure. The number distributions (**b**) of the fragments formed by both processes were very similar and adhere to a power law relation $N \propto d^{-f}$, where the exponent f is the fractal dimension

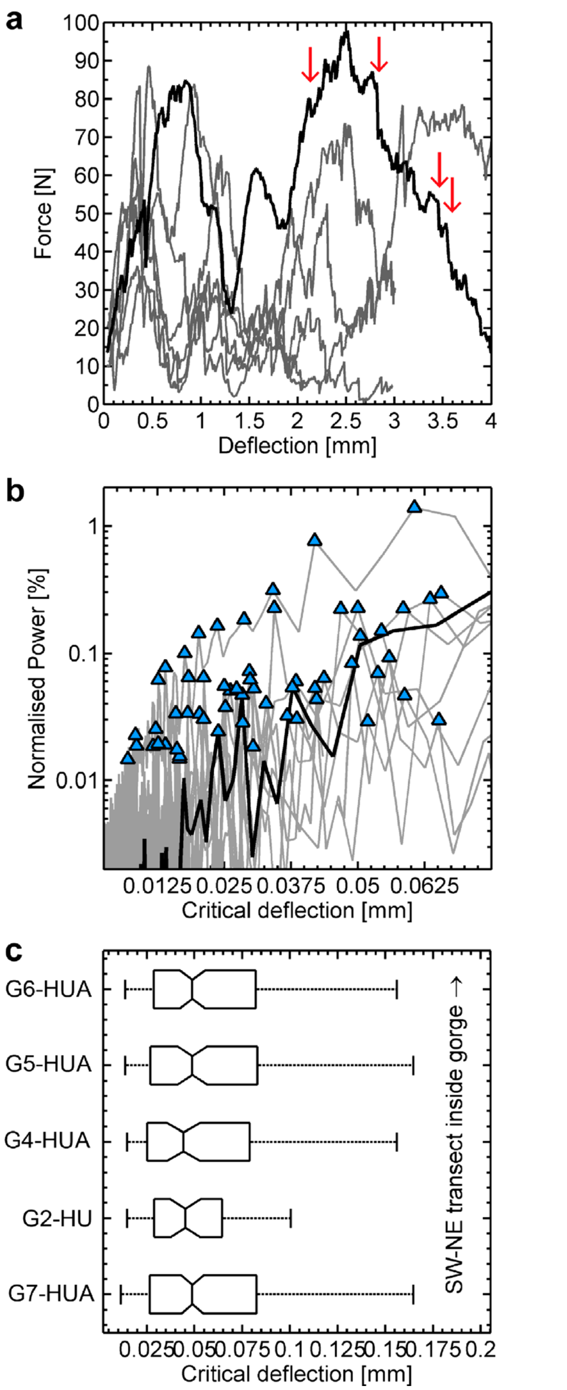

Fig. 6 Force signal analyses from the uniaxial loading of vesicular particles. An example is shown for data obtained from the fracturing of nine different clasts from location G2-HU. Image **a** shows the variable force measured at a given deflection (compression) of the particle. *Red arrows* highlight examples in the signal where a rapid decrease in the applied force signifies a fracturing event that was preceded by a momentary increase in force. Shown in **b** are the frequently occurring deflection distances (*peaks* marked with *blue triangles*) at which such minute fracturing events takes place. Based on these Fast Fourier Transform analyses, we determined the averages of these 'critical deflection' distances per sampled location, summarised by box plots in **c**. As the notches in the box plots overlap, it is a statistical indication that the critical deflections do not significantly differ

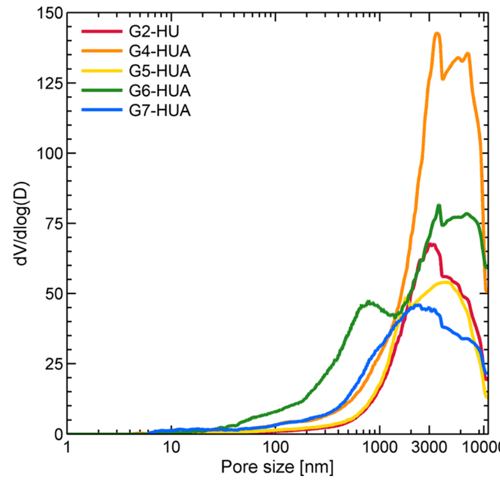

Fig. 7 A comparison of the porosity of vesicular hyaloclastite particles using high-pressure mercury intrusion. *Individual curves* are the average of nine independent repetitions (n=9) in which 10 individual vesicular fragments were used. Similar modes are visible, and the differences in vertical magnitude represent the volumetric abundance of a given pore diameter

In the second suite of experiments, the modification by particle transport was studied. The experiment parameters and transport distances of the sediment per drum are summarised in Table 3. As all available material was inserted in the drum, different starting weights are listed. After extraction of each aliquot the total weight decreased. After 15 weeks of tumbling (or 578–715 km of transport, see Table 3) the distributions of particle sizes showed no significant changes in the granulometry (Fig. 8). For the mode <10 μm, marginal broadening occurred, which was significant based on a comparison of the surface below the graph with a paired t test with $p \leq 10^{-3}$; but absolute values fall within the measurement accuracy.

Discussion

Dissipation of stress by fracturing

In comparison to the temperature regime at the time of magma fragmentation, the fracturing in a post-eruptive environment occurs mainly in cold, freezing conditions that results in brittle fracturing (i.e. no ductile deformation takes place during frost weathering). Secondary fracturing from the stress induced by ice growth was found to be a rapid and effective process to reduce individual vesicular particles to a range of far finer particle sizes (Fig. 4). Indications from the meteorological stations (Table 1) show that local temperature conditions are favourable for frost weathering; several tens of cycles may occur in field conditions, while less than 10 frost cycles were sufficient in the experiments to fracture vesicular particles. The granulometry of the frost weathering experiments

Table 2 Porosimetry data of vesicular glass particles obtained with high-pressure mercury intrusion according to the DIN 66133 standard

Porosimetry	Units	Field sample				
		G2-HU	G4-HUA	G5-HUA	G6-HUA	G7-HUA
Pore volume	$cm^3\ g^{-1}$	0.056	0.126	0.056	0.115	0.059
Specific surface area	$m^2\ g^{-1}$	0.18	0.39	0.21	0.69	0.71
Envelope density (0.1 MPa)	$g\ cm^3$	2.092	1.818	2.106	1.78	2.140
Apparent density (400 MPa)	$g\ cm^3$	2.367	2.344	2.383	2.22	2.450
Skeletal density	$g\ cm^3$	2.409	2.327	2.355	2.290	2.573
Accessible porosity	%	11.7	22.4	11.7	20.5	12.7
Inaccessible porosity	%	1.5	0.9	0.3	2.0	4.2
Pore diameters						
Normalised [a]	nm	1,558	1,401	1,534	686	375
Mean	nm	3,730	4,777	3,725	2,915	2,405
Modal	nm	3,234	4,684	3,690	4,750	2,366

Values are based on averages of nine independent repetitions (n=9) per sample site

[a] Defined as a ratio of the pore volume and specific surface area, $4V_p/S_a$

matched those of the fragments produced by the uniaxial compression and their number distributions were also found to have comparable fractal dimensions (Fig. 5b). The obtained value of 2.1 is also well in line with fractal dimensions in the range of 1.4–3.5 obtained in other studies (e.g. Turcotte 1986, 1989; Perugini and Kueppers 2012). As the power-law over-estimates and underestimates some parts of the data, it is clear that there are physical properties that control fragmentation to preferential grain sizes. The key concept here is the comparable way in which the glass responds to stress generated by the application of an external force. Irrespective of how this fractal nature is explained (i.e. probability-based or energy-based fragmentation; Perfect 1997), we argue on the basis of the comparable granulometries and fractal dimensions that the observed fragmentation of the glass reflects a fracturing property of these rhyolitic hyaloclastites.

In order to induce fracturing, the generated stress field needs to exceed the size of the smallest limiting weakness in the material (Scherer 1999). In the compression tests, we have seen that the applied stress can be sustained to deflections of 25–75 μm; we interpret this length scale as the size of the limiting weakness of the glass. A stress field generated by ice expansion thus needs to exceed a comparable magnitude of 25–75 μm to induce the type of fracturing shown in Fig. 4 and form the particle-size distributions in Fig. 5a. The required magnitude of this stress field can potentially be generated from the outside of the particle by the volumetric expansion of ice when it presses against the particle's exterior akin to the loading platens in the uniaxial compression experiments. This process would require voids of at least 1 mm in diameter where the 9 % volumetric expansion produces a radial expansion in the order of 25–75 μm. This dimension exceeds the size of all surficial pores by one or two orders of magnitude. However, voids between individual particles (i.e. interstitial voids from grain packing, perlitic fractures or the 10–20 % abundance of large, 1 mm diameter vesicles; Denton et al. 2012) can have sufficient volume to support this process. As rhyolitic hyaloclastites are poorly consolidated, ample voids will be available in the top layer and especially in less-compacted sedimentary deposits to facilitate this form of weathering.

Pores and internal damage

Detailed mercury intrusion measurements show that the modal pore diameters in Fig. 7 are a common property of the Grænagil particle population, characterised by surface pores >1,000 nm. Pore pressurisation during freezing of the Grænagil glasses is, therefore, favoured by the μm-sized surface pores that exceed the size of many small surface flaws formed by e.g. perlitisation of the glass (Fig. 9). Remarkably, no wide-spread fracturing was observed during mercury intrusion at pore pressures of 400 MPa (well-above the hydrostatic pressures created during freezing). This observation may be explained by the fact that mercury will provide an isotropic stress, i.e. from all sides of the particle, such that failure does not occur along a preferential fracture line. Frost weathering will generate an anisotropic (non-uniform) stress due to uneven freezing of the particle, which can induce the type of fracturing shown in Fig. 4. The process is also indiscriminative to the nature of the surface pore (i.e. a nanometre-sized hydration pits, micro-vesicle and cracks) as the physics of ice infiltration into these pores is similar and primarily dependent on the pore diameter (Scherer and Valenza 2005). For smaller particle sizes many frost cycles will be required to induce fracturing by pore pressurisation

Table 3 Data overview of the tumbling experiments and the conversion to field conditions

Sample	Parameters tumbling experiments				Field conditions
	Mass (g)	Height, *p* (cm)	Avalanche length (cm)	Duration (days)	Transport distance (km)
G4-HUA					
Week 1	178.2	3.9	9.7	6	43.1
Week 2	167.0	3.7	9.7	13	90.7
Week 3	155.7	3.6	9.6	20	141.2
Week 4	143.9	3.4	9.5	27	186.7
Week 5	132.1	3.2	9.3	34	233.7
Week 15	120.1	3.0	9.2	107	715.2
G5-HUA					
Week 1	192.1	3.9	9.7	6	43.1
Week 2	180.1	3.7	9.6	13	90.7
Week 3	168.0	3.5	9.5	20	141.0
Week 4	155.6	3.3	9.4	27	186.2
Week 5	143.2	3.1	9.2	34	232.8
Week 15	130.8	2.9	9.1	107	708.1
G6-HUA[a]					
Week 1	58.2	1.9	7.8	6	34.7
Week 2	58.2	1.9	7.8	13	73.3
Week 3	58.2	1.9	7.8	20	114.6
Week 4	58.2	1.9	7.8	27	152.3
Week 5	58.2	1.9	7.8	34	191.7
Week 15	48.5	1.7	7.6	107	588.6
G7-HUA					
Week 1	228.6	3.9	9.7	6	43.1
Week 2	214.1	3.6	9.6	13	90.4
Week 3	200.0	3.3	6.4	20	140.2
Week 4	185.0	3.0	6.2	27	184.5
Week 5	169.8	2.7	8.9	34	229.5
Week 15	155.9	2.5	8.6	107	681.4
G9-A[a]					
Week 1	74.7	1.9	7.8	6	34.7
Week 2	74.7	1.9	7.8	13	73.3
Week 3	74.7	1.9	7.8	20	114.6
Week 4	74.7	1.9	7.8	27	152.3
Week 5	74.7	1.9	7.8	34	191.7
Week 15	61.8	1.6	7.4	107	578.2
G1-A					
Week 1	193.1	3.9	9.7	6	43.1
Week 2	176.8	3.7	9.6	13	90.6
Week 3	163.3	3.4	9.5	20	140.8
Week 4	148.5	3.2	9.3	27	185.8
Week 5	134.8	3.0	9.2	34	232.0
Week 15	125.9	2.8	9.0	107	702.0

We assumed that each particle participated in at least one avalanche per revolution of the drum for determining the transport distance. The mass changed as a result of samples taken from the sediment inside the drum, without causing significant changes to the avalanche parameters

[a] Sampled in week 0, 5 and 15 due to availability of size fraction in field samples

as these grain sizes lack the larger vesicles and beneficiary particle packing that promote the effects of external damage.

Various lines of geological evidence support a glaciovolcanic setting for the hyaloclastite formation at Bláhnúkur and these include columnar joint orientations (Tuffen et al. 2001) and

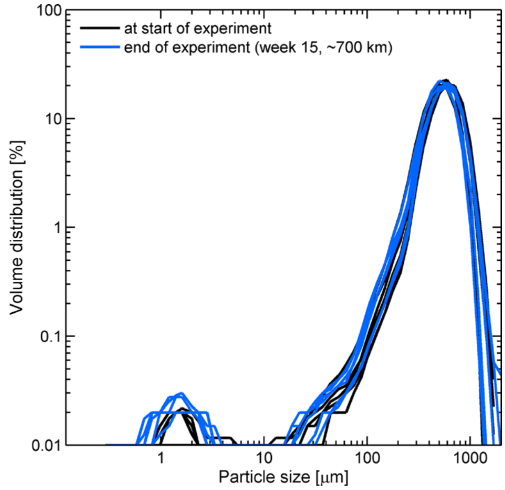

Fig. 8 Particle size distributions before and after prolonged down-slope transport. The rotational tumbling set-up (Fig. 2) was used to mimic the effects of particle rolling and avalanching down slope in dry conditions. Effects of abrasion are notably absent when comparing the distribution before (in *black*) and after 15 weeks (or 578–715 km of transport) of continuous axial tumbling (in *blue*). Modification at intermediate stages was insignificant in the first 1–5 weeks of tumbling and these curves have been omitted for clarity

the hydration of glass and perlitisation (Denton et al. 2012; Ferk et al. 2012). As the volatile content of Bláhnúkur glasses has been shown to depend on the subglacial cavity pressure (e.g. Tuffen et al. 2010; Owen et al. 2012), it suggests that some control was also exerted on the chemical parameters that

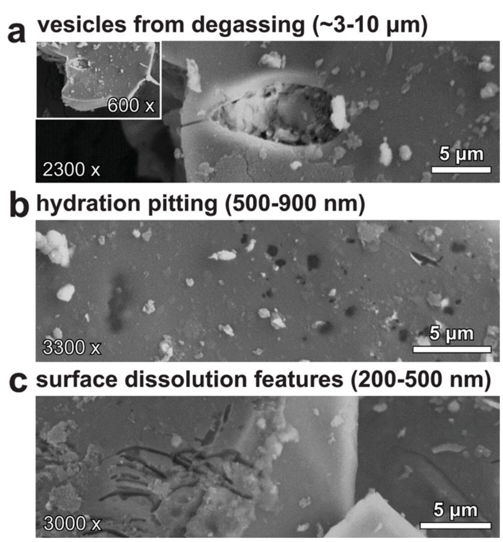

Fig. 9 Surface pores imaged using Back-Scattered Electron microscopy (BSE) of blocky ash shards from Grænagil. Different types of pores are characterised by their shapes and sizes, such as **a** vesicles formed by degassing, shown here for a blocky ash shard with adhering µm-scale glass fragments, **b** prominent dark pits on a shard surface that are indicative of hydration pitting, and **c** elongate pitted channels etched on the glass surface suggest local surface dissolution, which goes beyond hydration pitting. Pore diameters are given for the minor axis, which is the length-scale quantified using mercury intrusion (see Fig. 7). Images courtesy of H. Tuffen (modified from Tuffen 2001)

influence the viscosity and strength to resist syneruptive fragmentation (Martel et al. 2000; Owen et al. 2013). Surface porosity may therefore be controlled too by the eruption cavity conditions. Indications for a possible relation of glass porosity and eruption cavity conditions can be found in the trimodal distribution of pore diameters at sample site G6-HUA (Fig. 7). This additional mode at 700 nm can be interpreted as a result of hydration pitting processes related to the proposed steam filtering through these deposits during avalanching as suggested by Tuffen et al. (2001). Back-scattered electron microscopy of a quenched hyaloclastite fragment (Fig. 9) illustrate that 500–900 nm voids are indeed distinctively different from those formed by other alteration processes or from degassing during quenching of the glass. This also indicates that observed pore diameters >2,000 nm may be (at least partly) a property related to an earlier stage of magma degassing (i.e. exsolution of gasses), which occurred before or at the moment when the glass fragments quenched. We therefore postulate the idea that porosimetry may have interesting prospects for relating nm-µm pore diameters to syneruptive conditions and glass alteration processes.

In our discussion above, we have primarily addressed the mechanical effects of frost weathering using Bláhnúkur as a case study for processes that are more generally applicable to other (not necessarily subglacially formed) rhyolitic ash deposits elsewhere in Iceland. Other sites with rhyolitic ash deposits vary from nearby hyaloclastites at Dalakvísl (Owen et al. 2013) to those found at more distant outcrops at Hekla and Askja. Highly vesiculated ashes such as those found at Kerlingarfjöll (Stevenson et al. 2009) may even have a much greater potential for frost weathering due to their particle properties, compared to hyaloclastites exposed at Bláhnúkur. Future field studies may therefore be able to identify rates and volumes affected by these mechanisms by integrating observations of zones affected by frost weathering and measurements of seasonal denudation rates.

Abrasion during aeolian and gravity transport

Particle abrasions studies by Patel et al. (2013) showed that quenching of centimetre-sized pumice fragments did not greatly change their susceptibility to fracturing during transport processes (compared to non-quenched particles), although quenched particles were found to abraded slightly faster. The long duration and transport distances used in our tumbling experiments were, therefore, of a suitable magnitude for establishing if prolonged transport changes the granulometry of the ash matrix material due to abrasive effects. However, the quenched rhyolitic hyaloclastites in our study were found to be remarkably resistant to such particle abrasion. Changes to the sediment texture after prolonged transport were found only at the limit of detection. As particle abrasion is not dependent on the overlying mass in our experiment, but rather on the particle impact velocities (which are dependent on the avalanche length in the drum), effects of the changing volume due to aliquot extraction (Table 3) can be ruled out. The Grænagil gorge is ~2 km long, and the required transport distances for detectable modification thus exceed realistic transport distances that can be achieved in the field. We, therefore, conclude that frequently occurring low-energy transport regimes have little effect on the modification of rhyolitic hyaloclastites over time. Future high-energy abrasion experiments may provide more insight in the fracturing of ash textures and the evolution of their particle-size distributions, which can employ the experimental methods described by Merrison et al. (2010) and Marshall et al. (2012).

Health hazards

Fracturing of volcanic glass was found to produce fine silt-sized fragments, evidenced by a mode <10 μm (Fig. 5a) in the granulometry of the fragmentation products. This size range is noteworthy as it is easily suspended in the atmosphere by aeolian processes, which makes it a potential respiratory health hazard. Particle-size classes <10 μm are considered *thoracic* and upon respiration will primarily irritate upper airways (Horwell and Baxter 2006). The mode in Fig. 5 is found on ~2 μm, which makes this material *respirable*, i.e. it can enter deeper into the bronchia of the lungs where it can induce inflammatory responses, asthma and bronchitis (Horwell and Baxter 2006). De Vet and Cammeraat (2012) found that particle-size classes <63 μm are susceptible to deflation and can easily be suspended by moderate winds (<10 m s^{-1}) in dry conditions during summer. The higher frequency and timing of such events coincides with the main tourist season and this can potentially expose hikers on the trails across Bláhnúkur and through Grænagil to respirable ash. However, adverse effects are expected to be limited as these only occur after chronic exposure (Horwell and Baxter 2006) and the material lacks the crystalline phases of silica that make respirable ash particularly hazardous.

Iceland's sandy deserts have a high abundance of basaltic and rhyolitic volcanic glass and vesicular fragments that are continuously subjected physical weathering by Iceland's inland climate. Conditions favourable for large-scale dust suspension also occur frequently and they are notorious in the coastal areas (Arnalds 2010; Leadbetter et al. 2012). Such suspension events illustrate that the abundance and new generation of fine dust exceeds the rates of chemical weathering and soil uptake that would otherwise inhibit further distribution. Frost weathering of glass-rich eruption products thus contributes to the continuous formation of respirable dust, which in turn increases the potential health hazards associated with widespread dust-suspension events.

Assessments of health hazard after volcanic eruptions in subarctic or high-alpine periglacial environments have so far structurally overlooked the role of physical weathering in the secondary fracturing of glassy eruption products (e.g. Gudmundsson 2011, Carlsen et al. 2012). The processes identified in this study and the methods used to study them can, when combined with field observations of erosion rates or in-situ measurements of the frost weathering zone, provide complementary data for assessments of the long-term contribution of physical weathering to respirable dust generation after (subglacial) volcanic eruptions.

Concluding remarks

In contrast to basaltic volcanic glasses, rhyolitic hyaloclastites are not consolidated by chemical weathering. This makes rhyolitic glass much more susceptible to physical weathering and it promotes different pathways for the geomorphological development of landforms composed of rhyolitic glass. Laboratory simulations have allowed us to assess the scales, effects and characteristics of physical weathering of rhyolitic glaciovolcanic glass (summarised in Table 4) for processes that were observed in field conditions. Measurements of physico-mechanical properties can be used to understand the

Table 4 Summary of the scale effects and mechanisms contributing to the physical modification of rhyolitic hyaloclasts based on laboratory experiments presented in this study

Process	Location	Affected particle size (μm)	Process scale (μm)	Effects
Ice nucleation				
Volumetric expansion (external damage)	Interparticle pore space, perlite cracks, vesicles	>5,000	>25	Fracturing as means to dissipate an applied stress, production of many smaller grain sizes
Hydrostatic pressure (internal damage)	Surficial pores of individual particles	>10	>0.1–1	Propagation of cracks in glass and perlite, superficial fracturing
Abrasion during wind/gravity transport	Exposed particle surface	300–600	<10	Superficial abrasion, minor textural changes (potentially increased in higher energy transport regimes)

aptitude of glaciovolcanic glass for secondary particle-size reduction processes such as frost weathering and particle transport. Frost weathering primarily drives the formation of new sandy textures by fracturing of vesicular glass on relatively short time scales. The formed fragment distributions obey a fractal relation and show that the observed fragmentation is a material property of vesicular volcanic glass subjected to stress. Mercury intrusion measurements identified common pore diameters, which suggest that such stress may be generated by freezing of water in pores and pore networks at different scales, formed by syneruptive gas exsolution, hydration pitting and post-eruptive chemical alteration processes (perlitisation). In contrast to frost weathering, fracturing of smaller glass fragments through low-energy transport processes was found to play a neglectable role in the modification of rhyolitic hyaloclastites. Granulometric analyses of fine-grained ash therefore require careful consideration of the post-eruptive modification by physical weathering (most notably by frost cycling), which may cause an overestimation of the fine grain size fraction formed by syneruptive fragmentation processes.

Acknowledgements We thank the Icelandic Environment Agency and the Icelandic Institute of Natural History for their permission to carry out fieldwork and sample collection in the wonderful Fjallabak Nature Reserve and Lilja-Rut Víðisdóttir and Helga Garðarsdóttir of Ferðafélag Íslands for their hospitality and support during our fieldwork campaigns. Facilities for sediment analyses were provided by the Vrije Universiteit Amsterdam and were supported by Martine Hagen. We also thank Jan van Arkel for his microscopic photography, George Scherer and Donald Turcotte for providing insights into frost weathering and fractal fracturing and we kindly acknowledge the valuable review comments by Hugh Tuffen, Ulrich Kueppers and Michael Manga that helped to improve this manuscript.

References

Aranson IS, Tsimring LS (2006) Patterns and collective behavior in granular media: theoretical concepts. Rev Mod Phys 78:641–692. doi:10.1103/RevModPhys.78.641

Arnalds O (2010) Dust sources and deposition of aeolian materials in Iceland. Icel Agric Sci 23:3–21

Arnalds O, Gisladottir FO, Sigurjonsson H (2001) Sandy deserts of Iceland: an overview. J Arid Environ 47:359–371

Arnalds O, Gisladottir FO, Orradottir B (2012) Determination of aeolian transport rates of volcanic soils in Iceland. Geomorphology 167–168:4–12. doi:10.1016/j.geomorph.2011.10.039

Bagnold RA (1954) The physics of blown sands and desert dunes. Methuen and Co. Ltd., London

Blake S (1984) Magma mixing and hybridization processes at the alkali silicic Torfajökull central volcano triggered by tholeiitic Veiðivotn fissuring, south Iceland. J Volc Geotherm Res 22:1–31

Caballero L, Sarocchi D, Borselli L, Cárdenas AI (2012) Particle interaction inside debris flows: evidence through experimental data and quantitative clast shape analysis. J Volcanol Geoth Res 231–232:12–23

Carlsen HK et al (2012) A survey of early health effects of the Eyjafjallajökull 2010 eruption in Iceland: a population-based study. BMJ Open 2:e000343. doi:10.1136/bmjopen-2011-000343

Carpineri A, Pugno N (2002) Fractal fragmentation theory for shape effects of quasi-brittle materials in compression. Mag Concr Res 54(6):473–480

Chapman M et al (2000) Volcanism and ice interactions on Earth and Mars. In: Zimbelmann J, Gregg T (eds) Environmental effects on volcanic eruption: from the deep oceans to deep space. Kluwer Academic/Plenum Publishers, New York, pp 39–73

de Vet SJ, Cammeraat LH (2012) Aeolian contributions to the development of hillslopes and scree sediments in Grænagil, Torfajökull, Iceland. Geomorphology 175–176:74–85. doi:10.1016/j.geomorph.2012.06.023

Denton JS, Tuffen H, Gilbert JS, Odling N (2009) The hydration and alteration of perlite and rhyolite. J Geol Soc 166:895–904

Denton JS, Tuffen H, Gilbert JS (2012) Variations in hydration within perlitised rhyolitic lavas—evidence from Torfajökull, Iceland. J Volcanol Geotherm Res 223–224:64–73

Einarsson P, Sæmundsson K (1987) Earthquake epicenters 1982–1985 and volcanic systems in Iceland (map). In: Sigfússon I (eds) Í hlutarins eðli, Festschrift for Þorbjörn Sigurgeirsson. Menningarsjóður, Reykjavík

Eshel G, Levy GJ, Mingelgrin U, Singer MJ (2004) Critical evaluation of the use of laser diffraction for particle-size distribution analysis. Soil Sci Soc Am J 68:736–743

Ferk A, Denton JS, Leonhardt R, Tuffen H, Koch S, Hess K-U, Dingwell DB (2012) Paleointensity on volcanic glass of varying hydration states. Phys Earth Plant Inter 208–209:25–37

Friedmann GM, Sanders JE (1978) Principles of sedimentology. John Wiley and Sons, New York, pp 78–81

Frolava YV (2008) Specific features in the composition, structure, and properties of volcaniclastic rocks. Mosc Univ Geol Bull 63:28–37

Furnes H, Fridel eifsson IB, Atkins FB (1980) Subglacial volcanics—on the formation of acid hyaloclastites. J Volcanol Geoth Res 8:95–110

Gislason SR, Oelkers EH (2003) Mechanism, rates, and consequences of basaltic glass dissolution: II. An experimental study of the dissolution rates of basaltic glass as a function of pH and temperature. Geochem Cosmochim Acta 67:817–3832

Good RJ, Mikhail RSH (1981) The contact angle in mercury intrusion porosimetry. Powder Technol 29:53–62

Greeley R, Iversen JD (1985) Wind as a geological process on Earth, Mars and Venus. Cambridge Planetary Science Series. Cambridge Univ. Press, Cambridge

Gudmundsson G (2011) Respiratory health effects of volcanic ash with special reference to Iceland. A review. Clin Respir J 5:2–9. doi:10.1111/j.1752-699X.2010.00231

Hartmann WK, Thorsteinsson T, Sigurdsson F (2003) Martian hillside gullies and Icelandic analogs. Icarus 162:259–277

Hinkel KM (1997) Estimating seasonal values of thermal diffusivity in thawed and frozen soils using temperature time series. Cold Reg Sci Technol 26:1–15

Hiramatsu Y, Oka Y (1966) Determination of tensile strength of rock by compression test of an irregular test piece. Int J Rock Mech Min Sci 3:89–99

Horwell CJ, Baxter PJ (2006) The respiratory health hazards of volcanic ash: a review for volcanic risk mitigation. Bull Volcanol 69:1–24. doi:10.1007/s00445-006-0052-y

Jakobsson SP (1978) Environmental factors controlling the palagonitization of the Surtsey tephra, Iceland. Bull Geol Soc Denmark 27:91–105

Jakobsson SP, Gudmundsson MT (2008) Subglacial and intraglacial volcanic formations in Iceland. Jökull 58:179–196

Jakobsson SP, Moore JG (1986) Hydrothermal minerals and alteration rates at Surtsey volcano, Iceland. Geol Soc Am Bull 97:648–659

Jarosch A, Gudmundsson MT, Högnadóttir T, Axelsson G (2008) Progressive cooling of the hyaloclastite ridge at Gjálp, Iceland, 1996–2005. J Volcanol Geotherm Res 170:218–229

Jones JG (1969) Intraglacial volcanoes of the Laugarvatn region, southwest Iceland, I. Q J Geol Soc Lond 124:197–211

Jones JG (1970) Intraglacial volcanoes of the Laugarvatn region, southwest Iceland, II. J Geol 78:127–140
Jull M, Mackenzie D (1996) The effect of deglaciation of mantle melting beneath Iceland. J Geophys Res 101:21815–21828
Kaitna R, Rickenmann D (2007) A new experimental facility for laboratory debris flow investigation. J Hydro Res 45:797–810. doi:10.1080/00221686.2007.9521817
Kueppers U, Perugini D, Dingwell DB (2006) "Explosive energy" during volcanic eruptions from fractal analysis of pyroclasts. Earth Planet Sci Lett 248:800–807
Kueppers U, Putz C, Spieler O, Dingwell DB (2012) Abrasion in pyroclastic density currents: insights from tumbling experiments. Phys Chem Earth Parts A/B/C 45–46:33–39. doi:10.1016/j.pce.2011.09.002
Leadbetter SJ, Hort MC, Von Löwis S, Weber K, Witham CS (2012) Modelling the resuspension of ash deposited during the eruption of Eyjafjallajökull in spring 2010. J Geophys Res 117. doi:10.1029/2011JD016802
León y León CA (1998) New perspectives in mercury porosimetry. Adv Colloid Interf Sci 76–77:341–372
Licciardi JM, Kurz MD, Curtice JM (2007) Glacial and volcanic history of Icelandic table mountains from cosmogenic ^{3}He exposure ages. Quat Sci Rev 26:1529–1546
Maclennan J, Jull M, Mackenzie D, Slater L, Grönvold K (2002) The link between volcanism and deglaciation in Iceland. Geochem Geophys Geosys 3. doi:10.1029/2001GC000282 Art. No. 1062
Mandelbrot BB (1975) Stochastic models for the earth's relief, the shape and the fractal dimension of the coastlines, and the number-area rule for islands. Proc Natl Acad Sci USA 72:3825–3828
Mandelbrot BB (1982) The fractal geometry of nature. WH Freeman, New York, p 495
Manga M, Patel A, Dufek J (2011) Rounding of pumice clasts during transport: field measurements and laboratory studies. Bull Volcanol 73:321–333
Mangold N, Baratoux D, Arnalds O, Bardintzeff J-M, Platevoet B, Grégoire M, Pinet P (2011) Segregation of olivine grains in volcanic sands in Iceland and implications for Mars. Earth Planet Sci Lett 310:233–243. doi:10.1016/j.epsl.2011.07.025
Marshall JR, Bull PA, Morgan RM (2012) Energy regimes for aeolian sand grain surface textures. Sediment Geol 253–254:17–24. doi:10.1016/j.sedgeo.2012.01.001
Martel C, Dingwell DB, Spieler O, Pichavant M, Wilke M (2000) Fragmentation of foamed silicic melts: an experimental study. Earth Planet Sci Lett 178:47–58
Mathews WH (1947) "Tuyas", flat-topped volcanoes in northern British Columbia. Am J Sci 245(9):560–570
Matsuoka N, Murton J (2008) Frost weathering: recent advances and future directions. Permafrost Periglac 19:195–210. doi:10.1002/ppp.620
McGarvie D (2009) Rhyolitic volcano-ice interactions in Iceland. J Volcanol Geotherm Res 4:367–389
McGarvie DW, Burgess R, Tindle AG, Tuffen H, Stevenson JA (2006) Pleistocene rhyolitic volcanism at Torfajökull, Iceland: eruption ages, glaciovolcanism, and geochemical evolution. Jökull 56:57–75
Merrison JP, Gunnlaugsson HP, Jensen SK, Nørnberg P (2010) Mineral alteration induced by sand transport: a source for the reddish color of martian dust. Icarus 205:716–718. doi:10.1016/j.icarus.2009.09.004
Nesbitt HW, Young GM (1984) Prediction of some weathering trends of plutonic and volcanic rocks based on thermodynamic and kinetic considerations. Geochem Cosmochim Acta 48:1523–1534
Owen J, Tuffen H, McGarvie DW (2012) Using dissolved H_2O in rhyolitic glasses to estimate palaeo-ice thickness during a subglacial eruption at Bláhnúkur (Torfajökull, Iceland). Bull Volcanol 74:1355–1378. doi:10.1007/s00445-012-0601-5
Owen J, Tuffen H, McGarvie DW (2013) Pre-eruptive volatile content, degassing paths and depressurisation explaining the transition in style at the subglacial rhyolitic eruption of Dalakvísl, South Iceland. J Volcanol Geotherm Res 258:143–162. doi:10.1016/j.jvolgeores.2013.03.021
Patel A, Manga M, Carey RJ, Degruyter W (2013) Effects of thermal quenching on mechanical properties of pyroclasts. J Volcanol Geotherm Res 258:24–30. doi:10.1016/j.jvolgeores.2013.04.001
Peacock MA (1926) The volcano-glacial palagonite formation of Iceland. Geol Mag 6:385–399
Peltier LC (1950) The geographic cycle in periglacial regions as it is related to climatic geomorphology. Ann Assoc Am Geogr 40:214–236
Perfect E (1997) Fractal models for the fragmentation of rocks and soils: a review. Eng Geol 48:185–198
Perugini D, Kueppers U (2012) Fractal analysis of experimentally generated pyroclasts: a tool for volcanic hazard assessment. Acta Geophys 60(3):682–698
Pjetursson H (1900) The glacial palagonite formation of Iceland. Scot Geogr Mag 16:265–293
Rocchi V, Sammonds PR, Kilburn CRJ (2002) Flow and fracture maps for basaltic rock deformation at high temperatures. J Volcanol Geotherm Res 120:25–42
Rouquérol J, Avnir D, Fairbridge CW, Everett DH, Haynes JH, Pernicone N, Ramsay JDF, Sing KSW, Unger KK (1994) Recommendations for the characterization of porous solids. Pure Appl Chem 66(8):1739–1758
Russel JK, Edwards BR, Porritt L, Ryane C (2014) Tuyas: a descriptive genetic classification. Quat Sci Rev 87:70–81. doi:10.1016/j.quascirev.2014.01.001
Scherer GW (1999) Crystallization in pores. Cem Concr Res 29:1347–1358
Scherer GW, Valenza JJ II (2005) Mechanisms of frost damage. In: Young F, Skalny JP (eds) Materials science of concrete VII, 1st edn. Wiley, New York, pp 209–246
Schopka HH, Gudmundsson MT, Tuffen H (2006) The formation of helgafell, southwest Iceland, a monogenetic subglacial hyaloclastite ridge: sedimentology, hydrology and volcano-ice interaction. J Volcanol Geotherm Res 152:359–377
Sing KSW, Everett DH, Haul RAW, Moscou L, Pierotti RA, Rouquérol J, Siemieniewska T (1985) Reporting physisorption data for gas/solid systems with special reference to the determination of surface area and porosity. Pure Appl Chem 57(4):603–619
Slater L, Jull M, Mackenzie D, Grönvold K (1998) Deglaciation effects on mantle melting beneath Iceland: results from the Northern Volcanic Zone. Earth Planet Sci Lett 164:151–164
Smellie JL (2006) The relative importance of supraglacial versus subglacial meltwater escape in basaltic subglacial tuya eruptions: an important unresolved conundrum. Earth Sci Rev 74:241–268
Stevenson JA, Smellie JL, McGarvie DW, Gilbert JS, Cameron BI (2009) Subglacial intermediate volcanism at Kerlingarfjöll, Iceland: magma–water interactions beneath thick ice. J Volcanol Geotherm Res 185:337–351
Tuffen H (2001) Subglacial rhyolite volcanism at Torfajökull, Iceland. Unpublished PhD Thesis, Open University, UK
Tuffen H (2007) Models of ice melting and edifice growth at the onset of subglacial basaltic eruptions. J Geophys Res 112, B03203. doi:10.1029/2006JB004523
Tuffen H, Gilbert J, McGarvie D (2001) Products of an effusive subglacial rhyolite eruption: Bláhnúkur, Torfajökull, Iceland. Bull Volcanol 63:179–190
Tuffen H, Pinkerton H, McGarvie DW, Gilbert JS (2002a) Melting of the glacier base during a small-volume subglacial rhyolite eruption: evidence from Bláhnúkur, Iceland. Sediment Geol 149:183–198
Tuffen H, McGarvie DW, Gilbert JS, Pinkerton H (2002b) Physical volcanology of a subglacial-to-emergent rhyolitic tuya at Rauðfossafjöll, Torfajökull, Iceland. in: Smellie JL, Chapman MG

(Eds.), Volcano-ice interaction on Earth and Mars, Geological Society, London, Special publications 202, 213–236
Tuffen H, McGravie DW, Pinkerton H, Gilbert JS, Brooker RA (2008) An explosive-intrusive subglacial rhyolite eruption at Dalakvísl, Torfajökull, Iceland. Bull Volcanol 70:841–860
Tuffen H, Owen J, Denton J (2010) Magma degassing during subglacial eruptions and its use to reconstruct palaeo-ice thickness. Earth Sci Rev 99:1–18
Turcotte DL (1986) Fractals and fragmentation. J Geophys Res 91:1921–1926
Turcotte DL (1989) Fractals in geology and geophysics. P Appl Geophys 131(1–2):171–196
van Bemmelen RW, Rutten MG (1955) Tablemountains of Northern Iceland. Brill, Leiden, 217 pp
Walder JS, Hallet B (1986) The physical basis of frost weathering: toward a more fundamental and unified perspective. Arct Alp Res 18(1):27–32
Walker GPL (1965) Some aspects of quaternary volcanism in Iceland. Trans Leicester Lit Philos Soc 59:25–40
Whalley WB, Douglas GR, Jonsson A (1983) The magnitude and frequency of large rockslides in Iceland in the postglacial. Geogr Ann 65:99–110
Yang RY, Yu AB, McElroy L, Bao J (2008) Numerical simulation of particle dynamics in different flow regimes in a rotating drum. Powder Techol 188:170–177